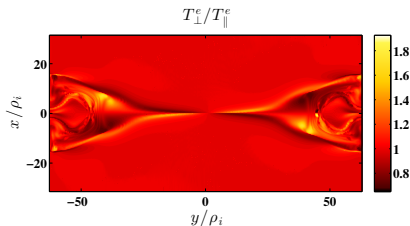


# Reconnection in Gyrokinetics Versus PIC in the Large Guide Field Limit

J. M. TenBarge, W. Daughton, H. Karimabadi, G. G. Howes,  
W. Dorland

March 2014



UNIVERSITY OF  
MARYLAND

# Can Gyrokinetics Really Capture Reconnection?

Magnetic reconnection is ubiquitous and plays an important role in energy transport.

- In-plane quantities play important role in determining reconnection physics, e.g., in-plane

$$\beta_y = 8\pi n_{0i} T_{0i} / \delta B_y^2 = \beta_i B_g^2 / \delta B_y^2 \sim \beta_i / \epsilon^2 \gg 1$$

- Produce density cavities and enhancements of order unity or greater
- Outflow velocities well in excess of the thermal speed, e.g.,

$$\frac{\delta v_e}{v_{te}} \sim \frac{d_e}{L} \frac{1}{\sqrt{\beta_i}} \frac{\delta B_0}{B_g} \sim \frac{\epsilon}{\sqrt{\beta_i}} \ll 1$$

- Significant temperature anisotropies
- Produce secondary instabilities such as firehose, Kelvin-Helmholtz, Bunemann

Despite this, many have studied gyrokinetic reconnection directly, e.g., [Rogers et al., 2007, Perona et al., 2010, Numata et al., 2010, 2011, Pueschel et al., 2011, Zocco and Schekochihin, 2011, Perona et al., 2012, Zacharias et al., 2012, Loureiro et al., 2013], but gyrokinetic reconnection has not been compared to full kinetic theory.

# Why Should We Care?

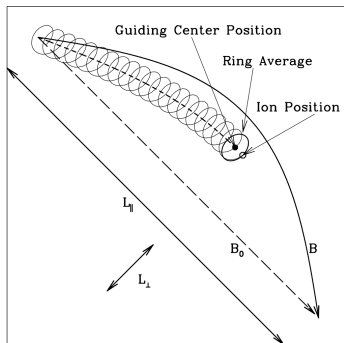
Turbulence naturally drives reconnection!

What is gyrokinetics?

- Average quantities over the gyro-motion of particles and describe the evolution of rings rather than particles
- Gyro-averaged and ordered version of full Vlasov-Maxwell kinetic theory
- Basic ordering parameters:  
$$\epsilon = \omega / \Omega_{ci} \sim \rho_i / L \sim k_{\parallel} / k_{\perp} \sim \delta B / B_g \ll 1$$

Why is it useful?

- Removes high frequency ( $> \Omega_{ci}$ ) fluctuations and reduces the problem from 6 to 5 dimensions
- Retains non-linear physics and kinetic effects (FLR, Landau damping, collisions)



<sup>1</sup>[Rutherford and Frieman, 1968, Taylor and Hastie, 1968, Antonsen and Lane, 1980, Frieman and Chen, 1982, Howes et al., 2006]

Relies on separations of time and spatial scales

- Low amplitude fluctuations:  $F = F_0 + \delta f$ , where  $\delta f \sim \epsilon F_0$
- Time scales,  $\tau^{-1} \ll \omega \ll \Omega_{ci}$ 
  - Fluctuations:  $\frac{1}{\delta f} \frac{\partial \delta f}{\partial t} \sim \omega \sim \epsilon \Omega_{ci}$
  - Transport:  $\frac{1}{F_0} \frac{\partial F_0}{\partial t} \sim \tau^{-1} \sim \epsilon^2 \Omega_{ci}$
- Spatial scales,  $\rho_i/L \sim \epsilon$ :
  - Perpendicular to  $B_g$ :  $\frac{\nabla_{\perp} \delta f}{\delta f} \sim 1/\rho_i$
  - Parallel to  $B_g$ :  $\frac{\nabla_{\parallel} \delta f}{\delta f} \sim 1/L$

# Consequences of The Gyrokinetic Ordering

- Cyclotron, plasma wave, and the fast magnetosonic branch are ordered out of system
- Subsonic drifts:  $v_d \sim \epsilon v_t$
- In the absence of collisions, magnetic moment fully conserved
- Rigorously quasi-neutral, i.e.,  $\delta n_i = \delta n_e$
- Must choose an  $\epsilon$  to connect to reality
- Most codes do not evolve the transport time-scale, i.e., the background does not evolve.

# PIC GK Comparison [TenBarge et al., 2013]

To address these issues, we set up nearly identical 2D reconnection simulations in NPIC/VPIC and AstroGK and compare.

## Basic parameters

- Fusion relevant  $\beta_i = 8\pi n_{0i} T_{0i} / B_g^2 = 0.01$  and solar wind relevant  $\beta_i = 1$  held fixed.
- PIC sweeps the reconnecting field,  $\delta B_0$ , down to achieve  $B_g = 5, 10, 20$ , and 50 times  $\delta B_0$  for  $\beta_i = 0.01$  and  $B_g = 1, 5$ , and 10 for  $\beta_i = 1$ .
- $m_i/m_e = 25$ ,  $\omega_{pe}/\Omega_{ce} = 0.8$
- Note that this means we are in the “non-dispersive” regime of inertial Alfvén waves for  $\beta_i = 0.01$ .
- For  $\beta = 0.01$ :  $L_x = L_y = 40\pi\rho_i$ ,  $w = 2\rho_i$ ,  $n_x = n_y = 1024$  or 2048,  $n_p = 1000$ ,  $n_e = 16$ , and  $n_\lambda = 32$
- For  $\beta = 1$ :  $L_x = L_y = 20\pi\rho_i$ ,  $w = \rho_i$ ,  $n_x = n_y = 2560$ ,  $n_p = 2000$ ,  $n_e = 8$ , and  $n_\lambda = 16$

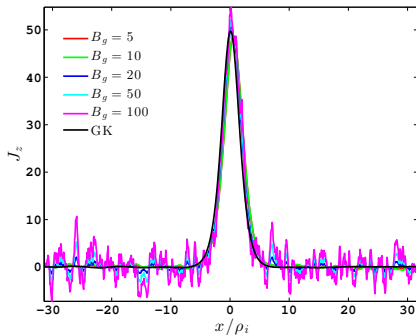
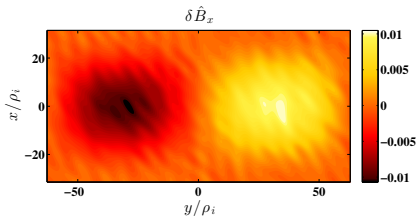
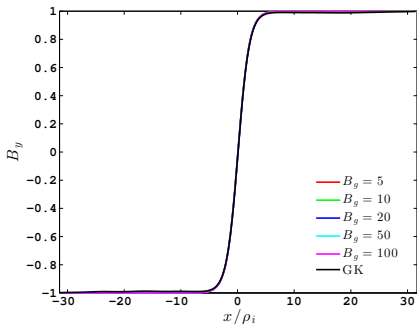
# Initial Conditions

Initial force-free magnetic field

$$\mathbf{B} = \delta B_0 \tanh(x/w) \hat{\mathbf{y}} + \sqrt{B_g^2 + \delta B_0^2 \cosh^{-2}(x/w)} \hat{\mathbf{z}}$$

with a 1% GEM perturbation

$$A_z = \delta B^{pert} \cos(2\pi x) \sin^2(2\pi y)$$



Out-of-plane current,  $J_z$ . PIC results have 10 point boxcar average applied.

# Force-free Versus Harris and Gyrokinetics

A Harris sheet is not initializable in GK.

In a Harris sheet, the current carrying particles are distinct from the background:

$$\begin{aligned} F &= F_M + \delta n(x) \exp [v_{\perp}^2 + (v_z - \delta U_z)^2] \simeq F_M + \delta n(x) F_M (1 - 2v_z \delta U_z + \dots) \\ &\simeq F_M [1 + \delta n(x)]. \end{aligned}$$

No current in GK for the typical Harris distribution!

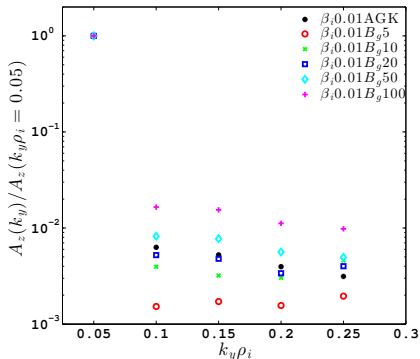
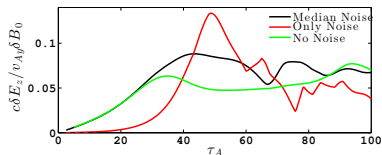
Whereas, in a force-free current sheet there is no perturbed density associated with the current

$$\begin{aligned} F &= n_0 \exp [v_{\perp}^2 + (v_z - \delta U_z(x))^2] \simeq F_M (1 - 2v_z \delta U_z + \dots) \\ &\simeq F_M [1 - 2v_z \delta U_z(x)], \end{aligned}$$

and we now have current in GK.

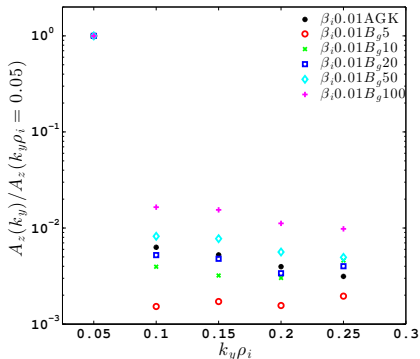
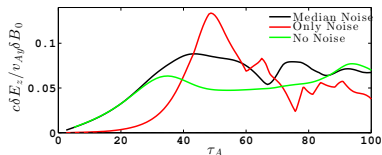
# We Also Add Noise to Match NPIC

- Populate first 20 Fourier modes in  $\hat{x}$  and  $\hat{y}$  with uniform random noise of equal RMS amplitude in  $B$ .
- Noise effects morphology and transient reconnection rate.



# We Also Add Noise to Match NPIC

- Populate first 20 Fourier modes in  $\hat{x}$  and  $\hat{y}$  with uniform random noise of equal RMS amplitude in  $B$ .
- Noise effects morphology and transient reconnection rate.

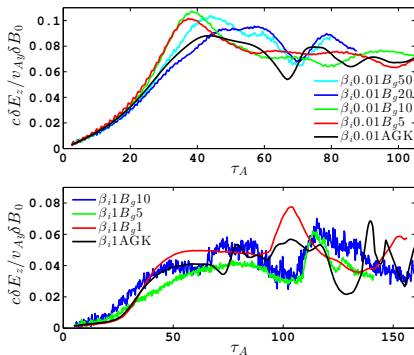


# Temporal Evolution

Purely noise

No noise

# Reconnection Rates

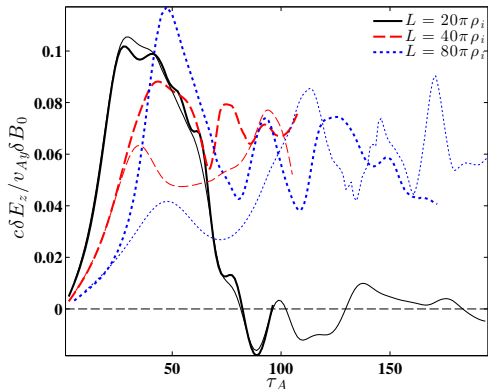


Reconnection rates as a function of in-plane Alfvén crossing time. Upper panel is  $\beta_i = 0.01$  and lower is  $\beta_i = 1$ .

- Note that for  $\beta_i = 0.01$  that  $\beta_i < m_i/m_e$ , i.e., no dispersive waves.
- Reconnection appears fast in the dispersiveless regime, which is not observed in two fluid codes.

# Scaling Study

That reconnection remains fast in the dispersiveless regime requires further evidence in the form of a scaling study—we alter the size of the simulation while keeping all other parameters fixed.



Thick lines represent runs seeded with noise.

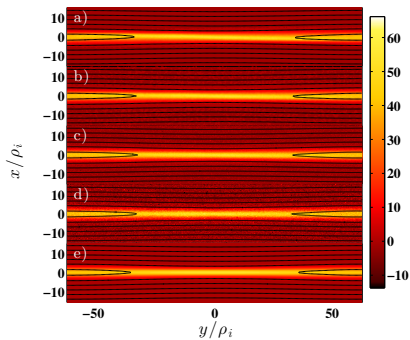
The peak rates seems to be box size independent, and the late-time, steady rate is box and noise independent above the flux limited threshold.

## Choosing an $\epsilon$

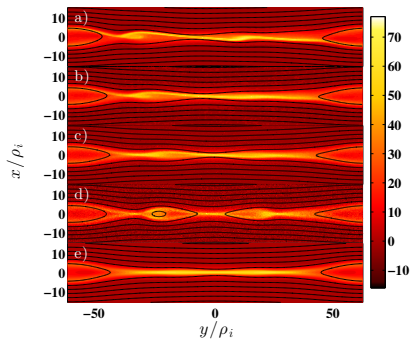
AstroGK quantities are normalized to  $\epsilon$ , e.g.,  $\delta B^{AGK} = \frac{\delta B}{B_g} \frac{1}{\epsilon}$ . To connect to the background quantities, we need to determine a value of  $\epsilon$ . We take  $\epsilon = \delta B_0 / B_g$  from PIC. Using this value for  $\epsilon$ , we can either convert PIC results to AGK normalization or vice versa.

For the following set of figures, the out-of-plane current from PIC has been converted to AGK units:  $J^{AGK} = \frac{J}{q_i n_{0i} v_{ti}} \frac{1}{\epsilon}$ .

# Early Time Current Comparison, $\beta_i = 0.01$

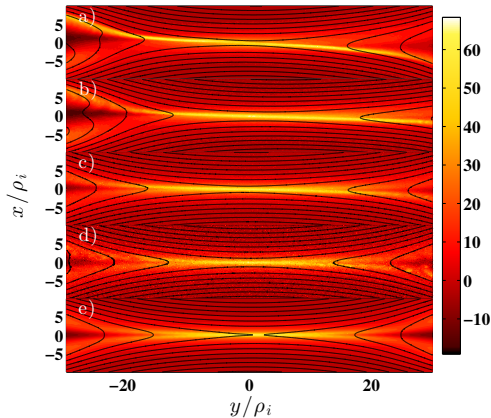


$J_z$  at  $\tau_A = 20$ : early, linear phase

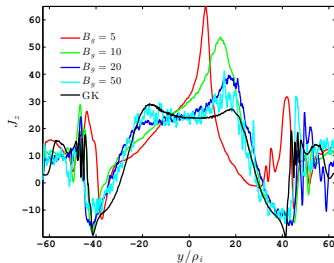
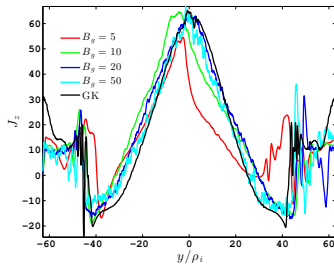


$J_z$  at  $\tau_A = 40$ : near peak reconnection

# Late Time Current Comparison, $\beta_i = 0.01$

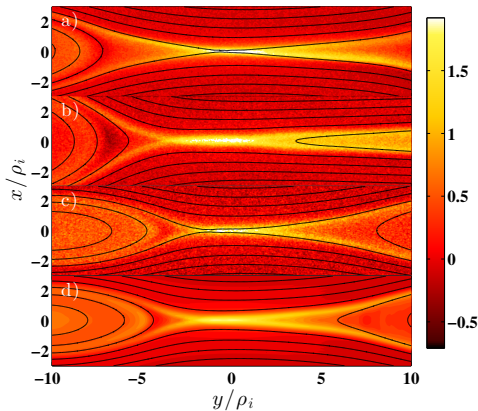


$J_z$  at  $\tau_A = 80$ : well after peak, dominated by physics



Cuts across  $J_z$  at  $x = 0$   
(upper) and  $x = -\rho_i$  (lower) at  
 $\tau_A = 80$ .

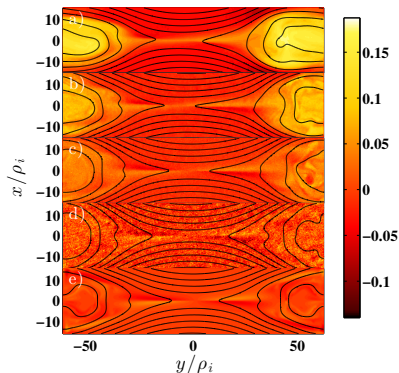
# Late Time Current Comparison, $\beta_i = 1$



$J_z$  prior to secondary island formation,  
 $\tau_A = 88, 90, 64,$  and  $73$ .

- $\beta_i = 0.01$  requires  $B_g/\delta B_0 \simeq 50$  to reach morphological convergence with GK.
- But,  $\beta_i = 1$  is converged by  $B_g/\delta B_0 = 5$ .
- So, the convergence has a clear  $\beta_i$  dependence.

# Morphology



$\delta B_z$  at  $\tau_A = 80$ : well after peak,  
dominated by physics

Pressure balance across the sheet  
implies

$$\delta P^{tot} + B_g \delta B_z / 4\pi + \delta B^2 / 8\pi = const.$$

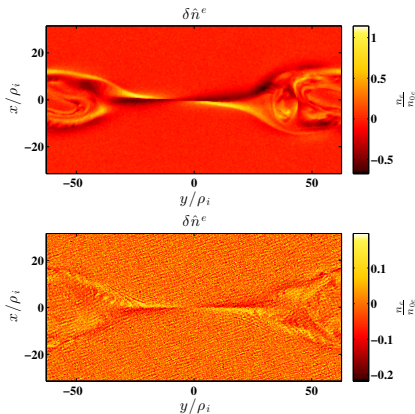
$\delta P^{tot}$  is well observed to have  
quadrupolar asymmetry for  $B_g >$   
 $0$  and  $\delta B^2$  is manifestly even.  
Assuming  $\delta P / P_0 \sim \delta B_0 / B_g$ ,

$$\frac{\delta B_z^{odd}}{\delta B_z^{even}} \sim \beta_i \frac{B_g}{\delta B_0} \sim \frac{1}{\epsilon}.$$

Therefore, the symmetry of  $\delta B_z$   
is determined by the above ratio  
Rogers et al. [2003]. Further,  $\delta B_z$   
and  $\delta n_e$  are anti-correlated along  
the separatrices, and  $J_z$  peaks at  
density enhancements.

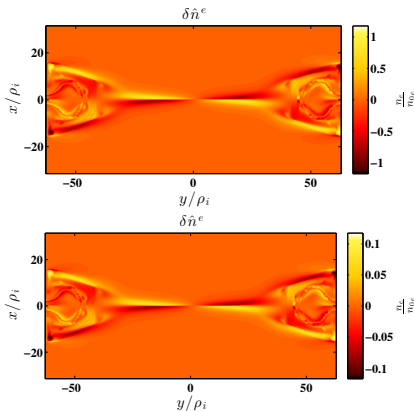
# Magnitude Comparison, Density

PIC



Perturbed electron density from PIC for  $B_g = 5$  (upper) and  $B_g = 50$  (lower).

AGK



Perturbed electron density from AstroGK assuming  $\epsilon = 1/5$  (upper) and  $1/50$  (lower).

# Magnitude Comparison

Ratios of the RMS of each value from PIC to the RMS AstroGK value over the regions presented in "Late Time Current Comparison" figures.

Run	$J_z$	$v_z^i$	$v_y^e$	$B_x$	$n_e$	$(T_{\perp}/T_{\parallel})^i$	$(T_{\perp}/T_{\parallel})^e$
$\beta_i 0.01 B_g 5$	1.1	1.2	0.90	1.0	0.92	0.97	0.012
$\beta_i 0.01 B_g 10$	1.1	1.2	0.94	0.93	0.98	1.0	0.95
$\beta_i 0.01 B_g 20$	1.0	1.2	1.0	0.85	1.1	1.0	0.99
$\beta_i 0.01 B_g 50$	1.0	1.5	2.4	0.95	2.0	1.0	1.0
$\beta_i 1 B_g 1$	1.1	1.4	1.1	1.0	1.3	0.84	0.92
$\beta_i 1 B_g 5$	1.1	1.4	1.1	1.2	1.3	0.99	1.0
$\beta_i 1 B_g 10$	1.1	0.98	1.1	0.99	1.8	1.0	1.1

# Temperature Anisotropy

$$P_{\parallel} = m \int d\mathbf{v} f v_{\parallel}^2 = P_{xx} \hat{b}_x^2 + P_{yy} \hat{b}_y^2 + P_{zz} \hat{b}_z^2 + 2P_{xy} \hat{b}_x \hat{b}_y + 2P_{xz} \hat{b}_x \hat{b}_z + 2P_{yz} \hat{b}_y \hat{b}_z = P_0 + \delta P_{zz} + 2 \frac{\delta B_z}{B_g} P_0$$

$$P_{\perp} \simeq \frac{P_{ii} - P_{\parallel}}{2} = P_0 + \frac{1}{2} (\delta P_{xx} + \delta P_{yy}) - \frac{\delta B_z}{B_g} P_0$$

And,

$$\frac{T_{\perp}}{T_{\parallel}} = \frac{T_0 + \delta T_{\perp}}{T_0 + \delta T_{\parallel}} = \frac{1/\epsilon + \delta \hat{T}_{\perp}}{1/\epsilon + \delta \hat{T}_{\parallel}},$$

where  $\delta \hat{T} = \delta T / (T_0 \epsilon)$  is in AGK units and  $\epsilon = \delta B_0 / B_g$ .

# Linear Scaling

- The observed magnitude agreement implies that the reconnection produced quantities scale linearly with the guide field in the  $B_g > \delta B_0$  limit.
- For example,  $\frac{J_z}{en_0 v_{ti}} \frac{B_g}{\delta B_0} = \text{const.}$  and  $\frac{\delta n_e}{n_{0e}} \frac{B_g}{\delta B_0} = \text{const.}$
- This scaling implies a single large guide reconnection simulation can be scaled to represent a wide range of guide fields.

# Energy In Each System

- The background in AstroGK does not evolve. Generally, the background evolves on the slow transport timescale in gyrokinetics.
- The total energy in PIC is  $E = \frac{B^2}{8\pi} + \sum_s \frac{1}{2} m_s n_s \delta U_s^2 + \frac{3}{2} P_s$ .
- This quantity is well conserved in the PIC simulations but requires a choice of  $\epsilon$  for comparison to AGK.
- Without invoking an  $\epsilon$ , we can instead use the perturbed energy only

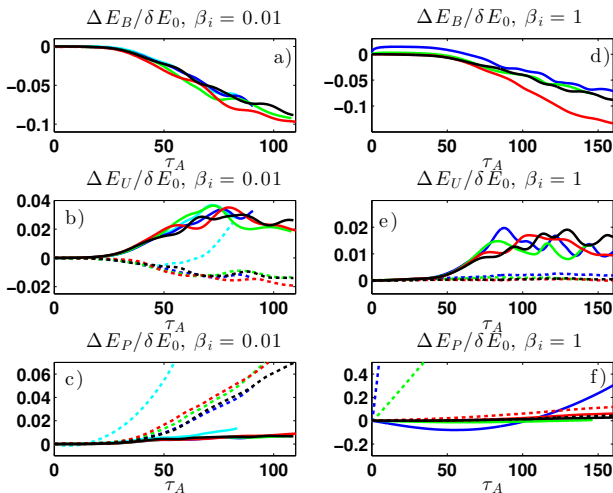
$$\delta E = \frac{\delta B^2}{8\pi} + \sum_s \frac{1}{2} m_s n_{0s} \delta U_s^2 + \frac{3}{2} \delta P_s.$$

- The conserved quantity in gyrokinetics is the generalized energy

$$W = \frac{\delta B^2}{8\pi} + \sum_s \int d^3\mathbf{v} \frac{T_{0s} \delta f_s^2}{2F_{0s}} = \frac{\delta B^2}{8\pi} + \sum_s \frac{1}{2} m_s n_{0s} \delta U_s^2 + \int d^3\mathbf{v} \frac{T_{0s} \delta \tilde{f}_s^2}{2F_{0s}},$$

where the final term is assumed to be equivalent to  $3\delta P_s/2$ .

# Energy Conversion



Plots of the change in the magnetic, a) and d), bulk kinetic, b) and e), and thermal, c) and f), energies from their initial values for  $\beta_i = 0.01$ , a)-c), and  $\beta_i = 1$ , d)-f). Solid lines indicate ion quantities and dashed are electron. All energies are normalized to the total initial energy in the system. Poor agreement of the electron thermal and bulk energies at high  $B_g$  is due to anomalous numerical dissipation in PIC.

# Summary

- PIC does converge morphologically toward gyrokinetics in the strong guide field limit, but the convergence is  $\beta_i$  dependent.
- Gyrokinetics makes correct predictions for the magnitudes of physical quantities, even outside its regime of formal applicability.
- Gyrokinetics fails to capture the correct morphology and secondary instabilities that arise for weaker guide fields.
- Reconnection quantities scale linearly with  $B_g$  in the  $\delta B_0 \ll B_g$  limit.
- The fractional energy change and anisotropic "heating" is well modeled by gyrokinetics for all values for which  $\delta B_0 < B_g$ .

# Bibliography I

- T. M. Antonsen, Jr. and B. Lane. Kinetic equations for low frequency instabilities in inhomogeneous plasmas. *Phys. Fluids*, 23:1205–1214, June 1980.
- M. A. Beer, S. C. Cowley, and G. W. Hammett. Field-aligned coordinates for nonlinear simulations of tokamak turbulence. *Phys. Plasmas*, 2:2687–2700, July 1995. doi: 10.1063/1.871232.
- E. A. Frieman and L. Chen. Nonlinear gyrokinetic equations for low-frequency electromagnetic waves in general plasma equilibria. *Phys. Fluids*, 25:502–508, March 1982.
- G. G. Howes, S. C. Cowley, W. Dorland, G. W. Hammett, E. Quataert, and A. A. Schekochihin. Astrophysical Gyrokinetics: Basic Equations and Linear Theory. *Astrophys. J.*, 651:590–614, November 2006. doi: 10.1086/506172.
- N. F. Loureiro, A. A. Schekochihin, and A. Zocco. Fast Collisionless Reconnection and Electron Heating in Strongly Magnetized Plasmas. *Phys. Rev. Lett.*, 111(2):025002, July 2013. doi: 10.1103/PhysRevLett.111.025002.
- R. Numata, G. G. Howes, T. Tatsuno, M. Barnes, and W. Dorland. AstroGK: Astrophysical Gyrokinetics Code. *J. Comp. Phys.*, 229:9347–9372, April 2010. doi: 10.1016/j.jcp.2010.09.006.
- R. Numata, W. Dorland, G. G. Howes, N. F. Loureiro, B. N. Rogers, and T. Tatsuno. Gyrokinetic simulations of the tearing instability. *Phys. Plasmas*, 18(11):112106, November 2011. doi: 10.1063/1.3659035.
- A. Perona, L.-G. Eriksson, and D. Grasso. Electron response to collisionless magnetic reconnection. *Phys. Plasmas*, 17(4):042104, April 2010. doi: 10.1063/1.3365518.
- A. Perona, D. Borgogno, and D. Grasso. Inertial magnetic reconnection effects on the electron dynamics in a three-dimensional configuration. *Journal of Physics Conference Series*, 401(1):012019, December 2012. doi: 10.1088/1742-6596/401/1/012019.
- M. J. Pueschel, F. Jenko, D. Told, and J. Büchner. Gyrokinetic simulations of magnetic reconnection. *Phys. Plasmas*, 18(11):112102, November 2011. doi: 10.1063/1.3656965.
- B. N. Rogers, R. E. Denton, and J. F. Drake. Signatures of collisionless magnetic reconnection. *J. Geophys. Res.*, 108:1111, March 2003. doi: 10.1029/2002JA009699.
- B. N. Rogers, S. Kobayashi, P. Ricci, W. Dorland, J. Drake, and T. Tatsuno. Gyrokinetic simulations of collisionless magnetic reconnection. *Phys. Plasmas*, 14(9):092110, September 2007. doi: 10.1063/1.2774003.

# Bibliography II

- P. H. Rutherford and E. A. Frieman. Drift Instabilities in General Magnetic Field Configurations. *Phys. Fluids*, 11: 569–585, 1968.
- J. B. Taylor and R. J. Hastie. Stability of general plasma equilibria - I formal theory. *Plasma Phys.*, 10:479–494, January 1968.
- J. M. TenBarge, W. Daughton, H. Karimabadi, G. G. Howes, and W. Dorland. Collisionless Reconnection in the Large Guide Field Regime: Gyrokinetic Versus Particle-in-Cell Simulations. *ArXiv e-prints*, December 2013. submitted to PoPL.
- J. M. TenBarge, G. G. Howes, W. Dorland, and G. W. Hammett. An Oscillating Langevin Antenna for Driving Turbulence Simulations. *Comp. Phys. Comm.*, 185:578, 2014.
- O. Zacharias, R. Kleiber, and R. Hatzky. Gyrokinetic simulations of collisionless tearing modes. *Journal of Physics Conference Series*, 401(1):012026, December 2012. doi: 10.1088/1742-6596/401/1/012026.
- A. Zocco and A. A. Schekochihin. Reduced fluid-kinetic equations for low-frequency dynamics, magnetic reconnection, and electron heating in low-beta plasmas. *Phys. Plasmas*, 18(10):102309, October 2011. doi: 10.1063/1.3628639.